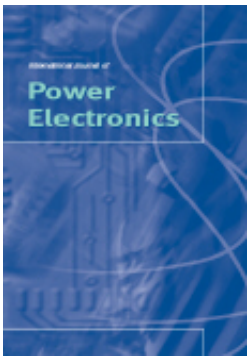

International Journal of Power Electronics

ISSN online: 1756-6398 - ISSN print: 1756-638X
https://www.inderscience.com/ijpelec

Less-rare-earth permanent magnet synchronous motor: a novel structure and its vibration analysis

Aiyu Gu, Mingjie Yang, Jianan Dong, Yongkang Ren

DOI: 10.1504/IJPELEC.2024.10056139

Article History:

Received:	12 August 2022
Last revised:	02 February 2023
Accepted:	01 April 2023
Published online:	23 December 2023

Less-rare-earth permanent magnet synchronous motor: a novel structure and its vibration analysis

Aiyu Gu*, Mingjie Yang, Jianan Dong and Yongkang Ren

Institute of Automation,
Guangdong University of Technology,
Guangzhou, Guangdong Province, China
Email: guay@gdut.edu.cn
Email: ymjcz3167@163.com
Email: 1932356335@qq.com
Email: 408853769@qq.com
*Corresponding author

Abstract: Limited by the high price and scarcity of rare-earth materials, the less-rare-earth permanent magnet synchronous motor (LRE-PMSM) is emerging as a promising candidate. To solve the irreversible demagnetisation of non-rare-earth permanent magnets in LRE-PMSM, a novel reverse salient less-rare-earth permanent magnet synchronous motor (RS-LRE-PMSM) is proposed in this paper, which is obtained by changing the structure of the rotor based on a certain widely used electric vehicles (baseline motor). Firstly, the deduction process of the RS-LRE-PMSM and its electromagnetic performances are given. Then, the analytical method and finite element method (FEM) are used to find the electromagnetic force waves that have a great influence on the vibration and noise of both motors. The vibration performance of the baseline motor and the RS-LRE-PMSM is also investigated by the comparative study method, and then a method to improve the vibration performance of the RS-LRE-PMSM is used.

Keywords: less-rare-earth; permanent magnet synchronous motor; reverse salient; vibration and noise; resonance.

Reference to this paper should be made as follows: Gu, A., Yang, M., Dong, J. and Ren, Y. (2024) 'Less-rare-earth permanent magnet synchronous motor: a novel structure and its vibration analysis', *Int. J. Power Electronics*, Vol. 19, No. 1, pp.99–114.

Biographical notes: Aiyu Gu received her BS, MS and PhD degrees in Electrical Engineering from the Harbin Institute of Technology, Harbin, China, in 1992, 1995 and 1998, respectively. She is currently an Associate Professor with the School of Automation, Guangdong University of Technology, Guangzhou, China. Her research interests include electric machines and control, and unconventional electromagnetic devices.

Mingjie Yang received his BS degree in Electrical and Intelligent Building from Fujian University of Technology, Fujian, China, in 2020. Currently, he is working toward his MS degree in Electrical Engineering at the School of Automation, Guangdong University of Technology, Guangdong, China. His research interests include the design and performance optimisation of motor structures.

Jianan Dong received his BS degree in Electrical Engineering and Its Automation from Shenyang University of Technology in 2019 and MS degree in Electrical Engineering from Guangdong University of Technology in 2022, respectively. His research interests include motor design.

Yongkang Ren received his BS degree in Electrical Engineering and its automation from Guangdong University of Technology, in 2019. He is currently working toward his MS degree in Electrical Engineering in the School of Automation, Guangdong University of Technology, Guangdong, China. His research interests include the optimal design of permanent magnet synchronous motor.

1 Introduction

Permanent magnet synchronous motors (PMSM) are widely used in military and electric vehicles (EVs) due to the advantages of high power density, high power factor and high efficiency (Xing et al., 2020; Dong et al., 2020). However, the price fluctuation and shortage of rare-earth permanent magnets (PMs) have limited the development and application of PMSM (Wang et al., 2018). Therefore, it has become an important indicator for motor manufacturers to reduce the number of rare-earth PMs. For this problem, researchers and scholars have started to pay attention to hybrid excitation permanent magnet motors (Boldea et al., 2014; Zeng et al., 2018; Zhu et al., 2019; Wang et al., 2019), which can significantly reduce the use of rare-earth and the manufacturing cost of motors. Therefore, an external rotor PMSM is proposed, and the rotor adopts U-shaped rare-earth PMs and arc-shaped non-rare-earth ferrite PMs to form a double-layer hybrid excitation structure (Ishii et al., 2012). Later, scholars have studied the characteristics of spoke-type permanent magnet motors and the results prove that this motor not only has better performance but also reduces the use of rare-earth materials (Kimiabeigi et al., 2015; Zhu et al., 2018). LRE-PMSM can maintain a certain power density while reducing the amount of PMs.

In the maximum torque per ampere (MTPA) control strategy, a negative d-axis demagnetisation current is used to increase speed. However, excessive demagnetisation currents can cause PMs demagnetisation for interior PMSMs, especially for non-rare-earth PMs (Poudel et al., 2021; Du et al., 2021). As a result, methods to reduce the demagnetisation current or increase the d-axis inductance have been proposed to combat this problem. As a result, methods to reduce the demagnetisation current or increase the d-axis inductance have been proposed to combat this problem. The authors first proposed two reverse salient less-rare-earth permanent magnet synchronous motors (RS-LRE-PMSMs) with different salient ratios for single and multi-layer fluxes (Bianchi and Bolognani, 1999; Bianchi et al., 2000). The comparative results show that the RS-LRE-PMSM requires only a small d-axis demagnetisation current to expand the speed and improves the irreversible demagnetisation of non-rare-earth materials. In recent years, scholars have proposed a q-axis external flux barrier method to convert the salient motor into reverse salient motor and have investigated the torque and anti-demagnetisation ability of both motors (Zheng et al., 2020, 2021). It is concluded that the RS-LRE-PMSM has better resistance to demagnetisation and overload. More authoritatively, the authors present three different rotor topologies for the LRE-PMSM

and compare the performance of the three motors and the results show that a spoke-type hybrid PMSM with parallel magnetic circuits is the best topology (Chen et al., 2020).

After verifying the feasibility of the electromagnetic performance of the motor, the vibration performance needs to be investigated as it has a significant impact on the performance of the whole machine. The vibration and noise of several motors with different pole-slot ratios are investigated and the effect of low order force waves on different motors is illustrated by using the finite element method (FEM) (Sun et al., 2011; Islam et al., 2014). The effect of pole-slot ratio and current saturation on air gap magnetic density harmonics is studied at the early stage of motor design, and the relationship between inherent mode and motor vibration is investigated (Kim et al., 2012). In the above studies, the researchers verified that the vibration and noise of the motor are related to the low order force waves and the inherent model. In the current study, in order to reduce the noise of the motor, the researchers mainly focused on the motor structure and the inverter. On the motor structure side, a method based on the armature teeth offset has been proposed, which results in a certain reduction in the maximum sound pressure level of the motor (Liu et al., 2021). On the inverter side, the authors consider the effect of inverters and inverter control strategies on motor vibration noise. Firstly, the researchers have theoretically derived the characteristics of radial electromagnetic forces and sideband current harmonics and used them to make adjustments to the waveform of the input signal, resulting in a reduction of more than 15dB in the vibration noise of the motor (Qiu et al., 2022).

This paper investigates and optimises the RS-LRE-PMSM and compares it with the baseline motor. The paper is organised as follows: at first, the deduction process of the RS-LRE-PMSM and the related electromagnetic performance of the motor are given. Then, the order and frequency of the radial force waves present in the motor are derived by analytical method and the finite element methods, as well as a low order inherent model for the motor. Finally, the method of magnets shifting is proposed to improve the vibration and noise the RS-LRE-PMSM.

2 Deduction process of the RS-LRE-PMSM and its electromagnetic performance

The ideal maximum speed that can be achieved by the motor can be written as:

$$\Omega_{\max} = \frac{u_{\lim}}{p\left(\varphi_f - L_d i_{\lim}\right)} \tag{1}$$

where $u_{\lim}$ and $i_{\lim}$ are the limited values of voltage and current, respectively; $\Omega_{\max}$ is the maximum speed that motor can reach under MPTA control strategy; φ_f correspond to the permanent magnet flux linkage; p is the pole pairs; L_d is the d-axis inductance.

According to (1), the maximum speed is limited by the inverter and is related to the magnetic flux linkage and the d-axis inductance. Therefore, for extending the speed range, a novel LRE-PMSM is initially proposed in this paper based on the baseline motor, as shown in Figures 1(a) and 1(b). In Figure 1(b), the flat-type rare-earth permanent magnets are segmented, while the spoke-type non-rare-earth permanent magnets are split, which not only increases the inductance of the d-axis, but also fully utilises the internal space of the rotor. Furthermore, to solve the risk of irreversible

demagnetisation of low coercive force PMs in LRE-PMSM, the method of adopting a non-uniform air gap and adding a q-axis flux barrier in the rotor is used to decrease the q-axis inductance, as shown in Figure 1(c). In the design process of the motor, the multi-objective optimisation method is used to determine the topology of the rotor, which will not be discussed in detail here. The specifications of the RS-LRE-PMSM are given in Table 1.

Figure 1 Deduction of the RS-LRE-PMSM, (a) baseline motor (b) LRE-PMSM (c) RS-LRE-PMSM (see online version for colours)

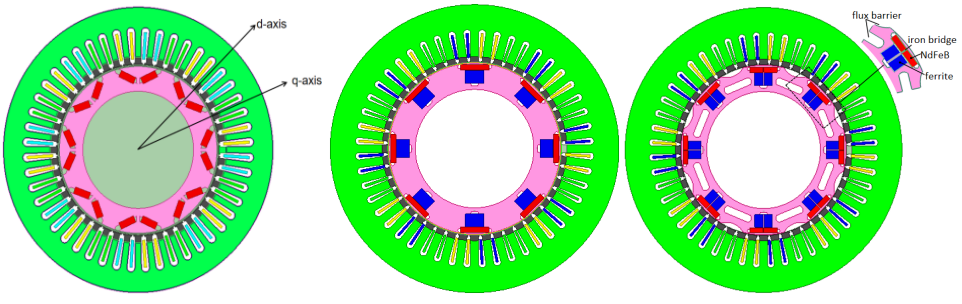

(a) (b) (c)

Table 1 Specifications of the RS-LRE-PMSM

Specifications	*Value*
Poles/slots	8/48
Outer diameter of stator (mm)	269.24
Inner diameter of stator (mm)	161.9
Outer diameter of rotor (mm)	160.4
Inner diameter of rotor (mm)	110.64
Air gap length (mm)	0.75
Axial length (mm)	83.32
Max phase current (A)	250
Rated speed (rpm)	3,000
Phase	3
Material	NdFeB/ferrite

For PMSM, the cost of PMs is a large part of the motor manufacturing cost. Therefore, the cost of PMs is considered in the design process of the RS-LRE-PMSM. The size and cost of the PMs of two motors are shown in Table 2 and the formula for calculating the cost of the PMs can be written as follows:

$$C_{Baseline} = 2l\rho_r w_{r1} P_r \tag{2}$$

$$C_{RS\text{-}LPM} = 2l\left(\rho_r w_{r2} P_r + \rho_f w_f P_r / k\right) \tag{3}$$

where $C_{Baseline}$ and $C_{RS\text{-}LPM}$ represent the cost of PMs in the baseline motor and RS-LRE-PMSM respectively; w, h and l are the width, thickness and axial length; P_r is the price of NdFeB; ρ_r = 7.5 g/cm^3, ρ_f = 4.9 g/cm^3; the subscripts $r1$, $r2$ represent the

NdFeB PMs in the baseline motor and RS-LRE-PMSM respectively, while *f* represents the ferrite PMs in the RS-LRE-PMSM; according to the long-term price of both materials in the market, the price of NdFeB is about 20 times that of ferrite, i.e., $k = 20$.

Table 2 Size and cost of PMs in the baseline motor and the RS-LRE-PMSM

Motor	*NdFeB (mm)*	*Ferrite (mm)*
Baseline motor	16 × 6.48	0
RS-LRE-PMSM	12.9 × 5	12 × 8

Figure 2 Torque of the baseline motor and the RS-LRE-PMSM (see online version for colours)

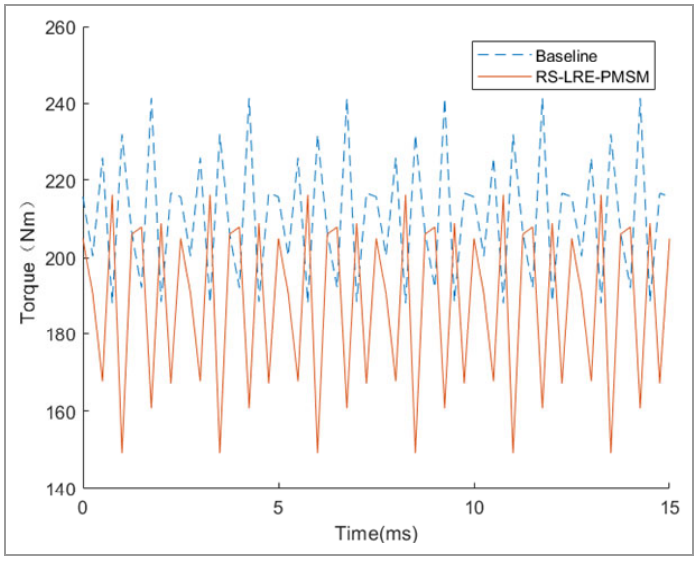

From the results in Table 2 and Figure 2, it is clear that the cross-sectional area of NdFeB can be significantly reduced and the electromagnetic torque can be maintained when the motor adopts the hybrid excitation method. In this RS-LRE-PMSM, the cost of PMs can be reduced by 34.8% and the average torque can be changed from 210.6 N·m to 187.9 N·m, which is a reduction of 10.1%. The unit cost torque of the baseline motor is 210.6 N·m, while that of the RS-LRE-PMSM is 289.1 N·m. Overall, while the average torque of the RS-LRE-PMSM is reduced by 10.1%, the unit cost torque is increased by 37.8%. To a certain extent, the RS-LRE-PMSM not only reduces the amount of rare-earth materials, but also improves the unit cost torque.

In summary, the RS-LRE-PMSM has the following characteristics:

1 The d-axis inductance is larger than the q-axis inductance, which is conducive to the flux weakening control, as shown in Figure 3.

2 The RS-LRE-PMSM is able to use a control strategy with a positive d-axis current below the base speed, and a wider speed range operation can be achieved above the base speed with a smaller q-axis demagnetisation current, which effectively avoids the risk of irreversible demagnetisation of low coercivity permanent magnets.

Figure 3 D- and q-axis inductance of the RS-LRE-PMSM (see online version for colours)

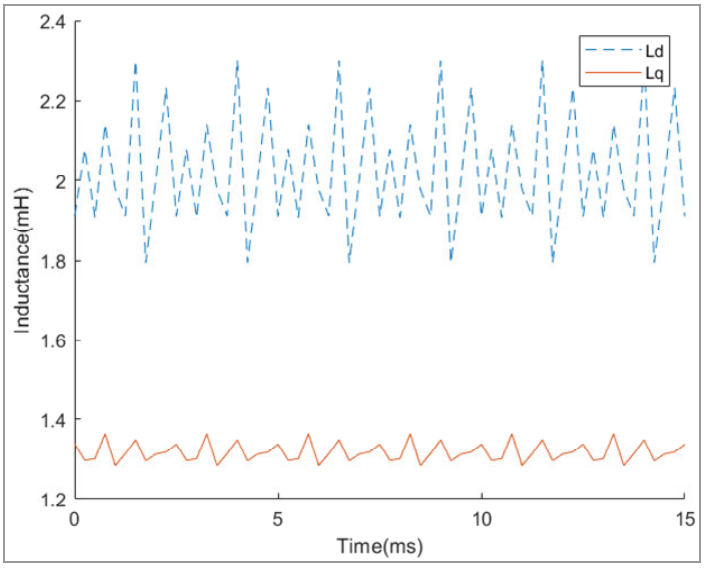

3 Analysis of electromagnetic force wave and modal structure

3.1 Analysis of electromagnetic force wave

The air-gap magnetomotive force (MMF) is generated by the rotor MMF and the stator MMF when the motor is running at rated speed. The air gap MMF and flux density can ideally be written as:

$$f(\theta, t) = F_u(\theta, t) + F_v(\theta, t) \tag{4}$$

$$b(\theta, t) = \lambda(\theta, t) \cdot f(\theta, t) \tag{5}$$

where $f(\theta, t)$ and $\lambda(\theta, t)$ are the air-gap MMF and permeability, respectively; θ is the spatial position angle.

The three main electromagnetic forces that cause electromagnetic vibration and noise in motors are Maxwell force, Laplace force and magnetostrictive force, among which Maxwell force plays an important role (Remus et al., 2020). Therefore, the radial electromagnetic force can be written as:

$$p_{rad} = \frac{b_r^2 - b_t^2}{2u_0} \tag{6}$$

where b_r and b_t are the radial air-gap flux density and tangential air-gap flux density, respectively; u_0 is the relative permeability of air.

Considering that b_t is much smaller than b_r, the radial force equation can be simplified by integrating (4)–(6):

$$p_{rad} \approx \frac{b_r^2}{2u_0} = \frac{(F_u(\theta,t)+F_v(\theta,t))^2 \cdot \lambda(\theta,t)^2}{2u_0} \tag{7}$$

By analysing the stator harmonic magnetic field and the rotor harmonic magnetic field of a 48-slot 8-pole PMSM, the waveform of the radial force and the corresponding frequency can be expressed as follows:

$$v = (2mk+1)p \tag{8}$$

$$u = (2r+1)p \tag{9}$$

$$r = u \pm v \tag{10}$$

$$f = (1 \pm u) f_0 \tag{11}$$

$$\Delta d \propto 1/r^4 \tag{12}$$

where k = 0, ±1, ±2, …; r = 0, 1, 2, …; u and v are the pole-pairs of the MMF harmonic of the rotor and stator, respectively; m is the number of phases; Δd is the amount of stator core deformation and ϒ is the radial force order.

According to (12), the deformation of the stator core is directly proportional to the 1/4 times of the radial force, which means that the low order radial forces have a greater effect on the vibration and noise. Therefore, this paper focuses on the radial forces of order less than 8. According to (8)–(11), the low order radial forces existing in the RS-LRE-PMSM in the ideal case are shown in Table 3. From the data in Table 3, the integer slot motor generates radial forces of 0 or 2p and does not generate radial forces of other orders in the ideal case.

Table 3 Radial force wave order of 48-slot-8-pole PMSM

v	u						
	4	*12*	*20*	*28*	*36*	*44*	*52*
4	0	8					
20		8	0	8			
28			8	0	8		
44					8	0	8
52						8	0

3.2 Mechanical modal structure analysis of stator

The vibration and noise of a certain PMSM is not only related to the amplitude, order and frequency of the radial forces, but also to the mechanical modal structure of the stator parameters. Studying the mechanical modal structure of the stator can avoid the frequency of its radial electromagnetic force wave from being similar to the inherent frequency of the stator mechanical modal structure during the motor design process; on the other hand, it can also study the inherent frequency of the stator and predict its actual vibration displacement and frequency response. Therefore, the modal structure analysis of the stator is an indispensable part of the analysis of the motor vibration and noise, which is an important method to study the structure of the motor from the dynamic point

of view. If the frequency of external excitation is close to or equal to the inherent frequency of the vibration mode will cause resonance, so the frequency will produce a large vibration and noise or may even cause damage to the motor and other problems. Generally speaking, there are two types of mechanical modal structure analysis methods, the first is the mechanical impedance theory method represented by the analytical method and the second is the FEM represented by the energy method.

When studying the vibration and noise of a PMSM using analytical methods, the motor can be approximated as a mechanical system. And the vibration equation can be written as:

$$[M]\{x''\}+[C]\{x'\}+[K]\{x\}=\{F\} \tag{13}$$

where $[M]$, $[C]$ and $[K]$ are the mass matrix, damping matrix and stiffness matrix, respectively. $\{x''\}$, $\{x'\}$ and $\{x\}$ are the acceleration, velocity and displacement vectors respectively. $\{F\}$ is the electromagnetic force vector.

When the energy method is used to analyse and calculate the inherent frequency of the stator, the Fourier series method and the FEM are commonly used. Although the Fourier series method is able to meet the exact calculation in engineering, for the case of complex mechanical modal structure of the stator, the Fourier transform method is more complicated compared with FEM. Therefore, in this article, FEM is used to analyse the vibration characteristics of the stator. Since the inherent frequency of the stator is related to the material properties, it is necessary to define the properties of the material such as the stator before using the FEM to calculate the inherent frequency of the stator. The relevant properties of the stator core and housing materials are given in Table 4.

Table 4 Material properties

Material	*Density (kg/m³)*	*Young's modulus (Mpa)*
Stator core	7,410	205,000
Housing	2,770	71,000

4 FEM and optimisation of the RS-LRE-PMSM

4.1 FEM

The vibration performance of the baseline motor and the RS-LRE-PMSM at rated speed are analysed by the FEM, and the radial electromagnetic force wave in the circumferential direction of the air gap and its Fourier transform are shown in Figures 4 and 5. From the results, the minimum order of the radial force wave is the greatest common divisor (GCD) of the number of poles-slots when core loss and other factors are not taken into consideration, which can be written as GCD (2p, Ns) (Yang and Chen, 2021). In Figure 4, although the radial forces of two motors have different phases, the number of periods of the force waves is the same. In Figure 5, the order of the forces obtained by Fourier transform is the same. This not only verifies the reliability of the analytical method, but also proves that the operating principle of the RS-LRE-PMSM is the same as that of the baseline motor. However, since the derivation of the analytical method is performed in the ideal case, while in the actual case due to many factors such as stator slotting and current harmonics, there are some radial force waves that do not

exist in the analytical method, such as the first, second and third order forces in Figure 5. Although their amplitude is small, they may also have an effect on motor vibration and noise. Taking the 1st order force wave as an example, if this force wave exists for a long time, the unbalanced magnetic pull generated by its long-term existence will shorten the service life of the rotating shaft and also generate large noise, so the effect of the low order force on vibration and noise should also be considered.

Figure 4 Air-gap radial force wave of two motors (see online version for colours)

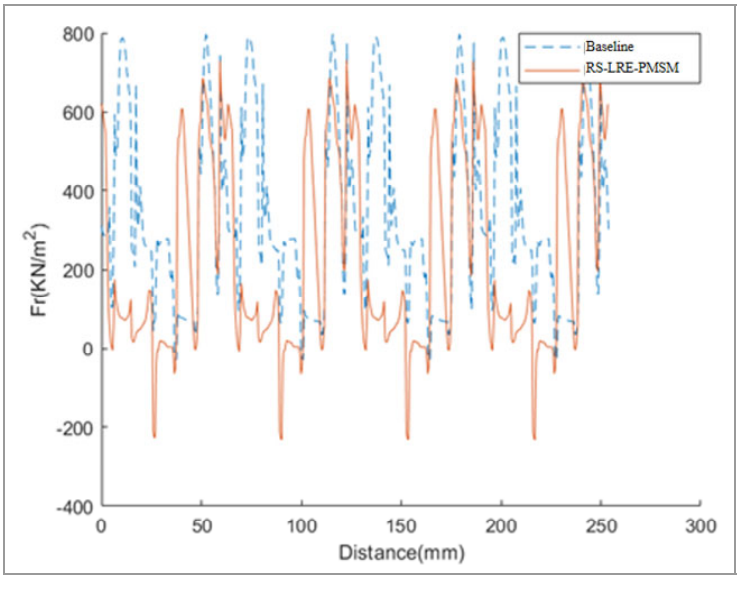

To further analyse the source of the vibration and noise of the motor, the stator teeth are separated from the stator yoke in the finite element software and the mesh of the stator teeth is dissected in more detail. The multi-speed noise sound pressure level (SPL) graph is derived by the finite element software as shown in Figure 6. The parts of the graph with maximum vibration and noise are also extracted and analysed for their corresponding force wave orders and frequencies, and the results are shown in Table 5 and Table 6. The radial force wave order and frequency is analysed when the baseline motor is running at 1,500 rpm, the force harmonic ($0.12f_0$) is mainly generated by two parts: the interaction of the 11th harmonic of the stator and rotor; and the interaction of the 13th harmonic of the stator and rotor. The results in Tables 5 and 6 show that the RS-LRE-PMSM has a maximum SPL of 95.4 dB at 6,000 rpm, compared to 89 dB at 3,500 rpm for the baseline motor. And except at 6,000 rpm, the SPL of the RS-LRE-PMSM at multi-speed is almost always lower than that of the baseline motor, which is a relatively good phenomenon. However, for the vibration and noise of the motor, the main concern is to reduce the maximum SPL, so the vibration and noise of the RS-LRE-PMSM needs to be further optimised.

Figure 5 Fast Fourier 2D transform of air-gap radial force wave (see online version for colours)

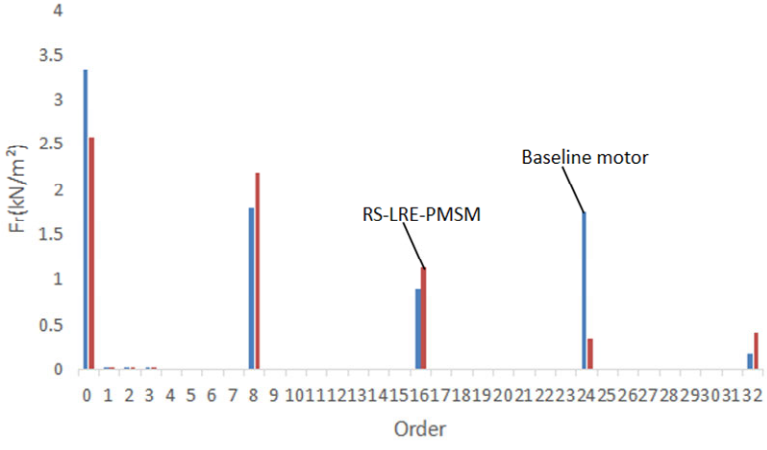

Figure 6 Multi-speed noise SPL diagram of two motors, (a) baseline motor (b) RS-LRE-PMSM (see online version for colours)

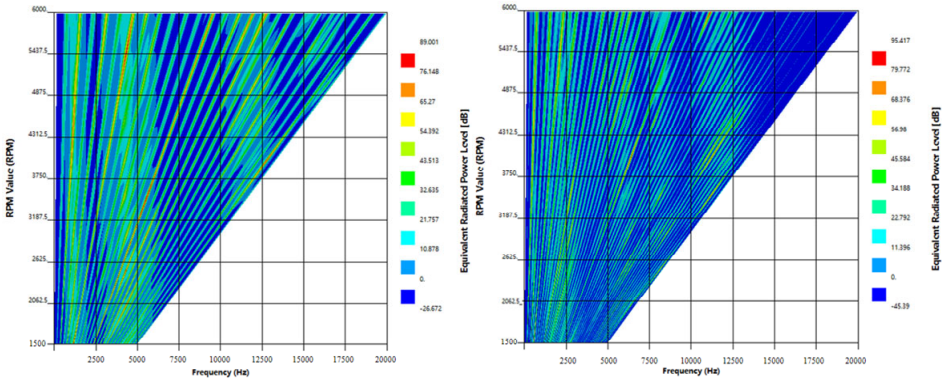

(a) (b)

Table 5 Force wave order and frequency of the maximum SPL at multi-speed of the baseline motor

Speed (rpm)	*Force order*	*Frequency (Hz)*	*SPL (dB)*	*Speed (rpm)*	*Force order*	*Frequency (Hz)*	*SPL (dB)*
1,500	0	1,200	82.4	4,000	0	12,800	83.2
2,000	8	4,266.67	80.1	4,500	8	1,200	74.8
2,500	8	4,333.33	81.4	5,000	0	4,000	70.7
3,000	0	4,800	76.8	5,500	0	4,400	83.4
3,500	0	5,600	89	6,000	0	12,000	77.4

Table 6 Force wave order and frequency of the maximum SPL at multi-speed of the RS-LRE-PMSM

Speed (rpm)	*Force order*	*Frequency (Hz)*	*SPL (dB)*	*Speed (rpm)*	*Force order*	*Frequency (Hz)*	*SPL (dB)*
1,500	0	600	70.5	4,000	0	6,400	85.5
2,000	8	2,133.33	60.8	4,500	8	600	73
2,500	0	2,000	58.5	5,000	8	1,333.33	42.8
3,000	8	2,800	65.8	5,500	0	2,200	70.2
3,500	0	11,200	82.9	6,000	8	11,200	95.4

Table 7 Low order inherent frequency of stator

Mode	*Frequency (Hz)*
2	1,243.5
3	2,964.2
4	4,704.4
5	5,612.9
5 (torsional vibration)	10,923

Figure 7 Motor low order vibration model, (a) 2nd order (b) 3rd order (c) 4th order (d) 5th order (e) front side (f) back side (see online version for colours)

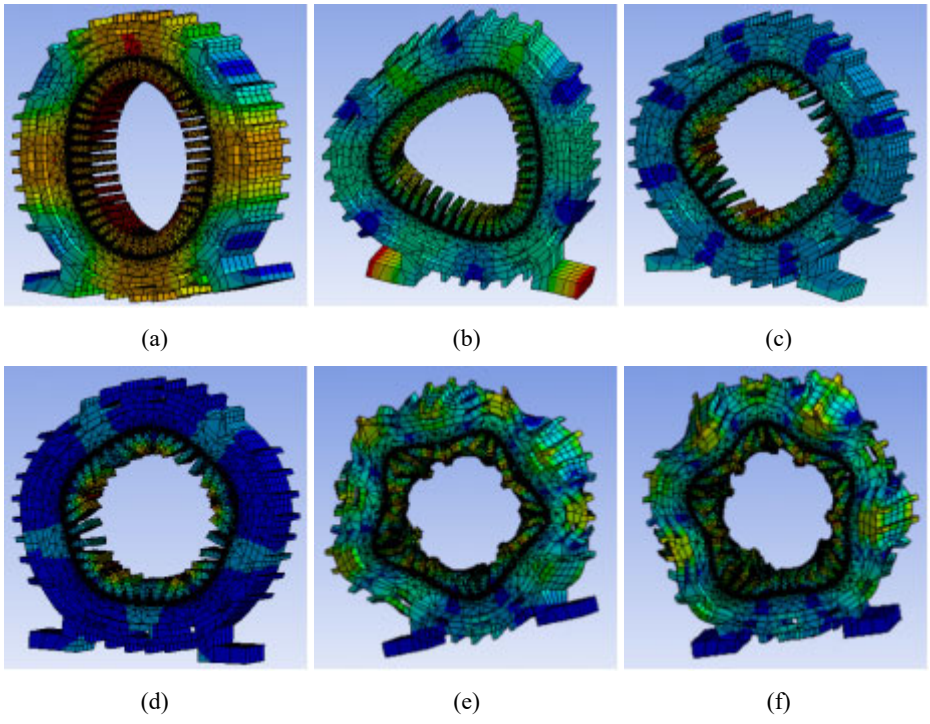

(a) (b) (c)

(d) (e) (f)

After defining the material of the stator and housing, the model is imported into the finite element software for analysis. The solved stator low order inherent frequency and vibration model are shown in Table 7 and Figure 7. According to Figure 6(a) and Table 7, the baseline motor has the highest SPL at 3,500 rpm, which corresponds to a frequency of 5,600 Hz. This frequency is similar to the inherent frequency of the 5th order mode of the stator and therefore generates a large amount of vibration and noise. According to Figure 6(b) and Table 7, the RS-LRE-PMSM has the highest SPL at 6,000 rpm, which corresponds to a frequency of 11,200 Hz. From the results in Figure 7(e) and Figure 7(f), the stator undergoes a 5th order modal forced torsional vibration near 11,200 Hz, which generates a large vibration and noise. Combining Tables 5, 6 and 7 for analysis, the maximum SPL of both motors is due to resonance resulting from the frequency of the radial force wave being close to the inherent frequency of the stator. Therefore, how to eliminate the maximum SPL has become a problem to be solved.

In general, the maximum SPL of a motor can be reduced by decreasing the amplitude of the radial force wave and increasing the stiffness of the material. Since the material of the motor must be selected according to the environment and purpose of the motor and other factors, there are certain limitations that make the selection difficult. For the previous method, reducing the radial force wave amplitude is simple and effective, so this method is used to optimise the maximum SPL of the motor.

4.2 Optimisation of the vibration and noise of the RS-LRE-PMSM

According to the above analysis combining radial force wave and vibration mode, the maximum SPL of the RS-LRE-PMSM is significantly different from the results obtained by the analytical method. That is, the effect of the tangential force wave on the vibration and noise of the RS-LRE-PMSM needs to be considered. The tangential force wave is generated by the torque ripple, while the torque ripple is related to the cogging torque, so this paper optimises the vibration and noise by optimising the cogging torque. According to Maxwell's stress tensor, the cogging torque of PMSM can be written as:

$$T_{cog} = \gamma^2 L_{ef} \int_0^{2\pi} \tau\left(\tau_c, \theta_c, t\right) d\theta_c \tag{14}$$

where γ_c is the average radius of the effective air-gap; L_{ef} is the effective axial length; $\tau(\tau_c, \theta_c, t)$ is the tangential electromagnetic force density at no-load.

For the motor with integer slot, the phase and amplitude of the cogging torque generated under each pole are the same (Leitner et al., 2019). Therefore, the total cogging torque of the motor is the sum of the cogging torque under each pole. The total cogging torque can be expressed as:

$$T_{cog} = \sum\nolimits_{k=1}^{\infty} T_k \sin\left(kN_s\theta + \varphi_k\right) \tag{15}$$

where k is the harmonic order of the cogging torque; T_k and φ_k are the amplitude and phase of the k^{th} cogging torque harmonic; θ is the rotor position angle; N_s is the number of stator slots.

From the above analysis it can be concluded that the cogging torque is related to the phase, amplitude and number of harmonics. Therefore, by changing the relative position of the PMs, the phase of the cogging torque under each pole is changed. Therefore, the equation for the cogging torque after magnets shifting can be written as:

$$T_{cog} = \sum_{h=0}^{N_{p-1}} \sum_{k=1}^{\infty} T_{pN_s k} \sin\left(kN_s\left(\theta - h\theta_0\right) + \varphi_k\right) \tag{16}$$

where $T_{pN_s k}$ is the amplitude of the cogging torque generated by one pole of the PM; θ_0 is the angle by which the two PMs are offset from each other.

The method of magnets shifting used in this paper is as follows: the first and fifth magnets are shifted θ, the second and sixth magnets are shifted $3/2\theta$, the third and seventh magnets are shifted $-3/2\theta$ and the fourth and eight magnets are displaced $-\theta$ (Dong et al., 2020), where θ is theoretical optimum offset angle, θ equals $(2\pi)/(N_s N_p)$, and the schematic diagram of magnets shifting is shown in Figure 8. After using the magnets shifting, the finite element software is used to generate the multi-speed waterfall diagram of the motor, and the results are shown in Figure 9. The force harmonic ($8.28f_0$) of the RS-LRE-PMSM has been reduced from 95.42 dB to 23.02 dB at the speed of 6,000 rpm after using magnets shifting, which is a reduction of 75.88%. And the maximum SPL at 6,000 rpm is 73.33 dB, which is a reduction of 23.15%. Moreover, the cogging torque and torque ripple are reduced while the average torque remains essentially unchanged. Although magnets shifting can reduce the effect of the tangential force wave on the motor, it may also aggravate the effect of lower order force waves on the whole machine. The maximum SPL corresponding to the three motors at different speeds and frequencies are shown in Table 8 and were obtained from the data in Figures 6 and 9.

Figure 8 Schematic diagram of magnets shifting (see online version for colours)

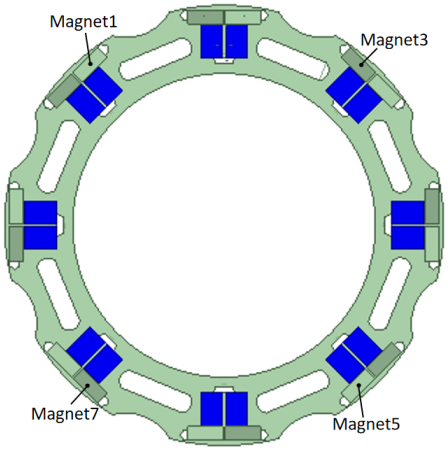

As can be seen from Table 8, the SPL of the RS-LRE-PMSM with magnets shifting is low in the high frequency band and its maximum noise SPL is reduced by 4.4% compared to the baseline motor and by 10.8% compared to the RS-LRE-PMSM. The results of the above analysis and optimisation show that the RS-LRE-PMSM with magnets shifting has better vibration performance.

Figure 9 Multi-speed waterfall diagram for the RS-LRE-PMSM after magnets shifting (see online version for colours)

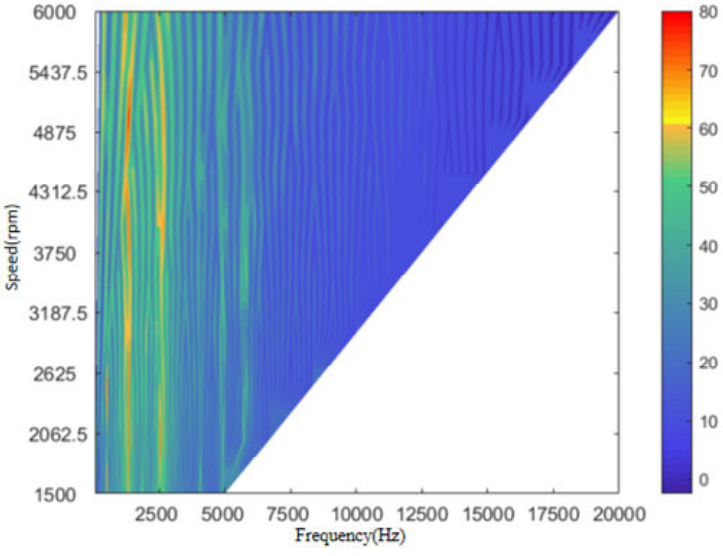

Table 8 The maximum SPL of the three motors at different speeds and frequencies,

Motor	*Speed (rpm)*	*Frequency (Hz)*	*SPL (dB)*
Baseline motor	3,500	5,600	89
Before shifting	6,000	11,200	95.42
After shifting	5,000	1,333.3	85.08

5 Conclusions

In order to solve a series of problems such as the cost of PMs in PMSM and the risk of demagnetisation of PMs in LRE-PMSM, this paper proposes a novel RS-LRE-PMSM with a 34.8% reduction in the cost of PMs. A brief comparison of two motors shows that the RS-LRE-PMSM not only maintains better electromagnetic performance, but also reduces the manufacturing cost of the motor. To further verify the feasibility of the RS-LRE-PMSM, the vibration and noise of the two motors are also compared at different speeds and frequencies. The results show that the RS-LRE-PMSM and the baseline motor share the same operating principle and produce the same radial force wave order. And further analysis and optimisation shows that the reason for the high noise SPL of the motor is due to resonance. In order to solve this problem, the maximum noise SPL of the RS-LRE-PMSM is effectively reduced by using magnets shifting method based on Maxwell's force equation.

Although the method of magnets shifting can reduce the maximum noise SPL of the motor to a certain extent, the unbalanced magnetic pulling force (i.e., first order force wave) that generated by this method may reduce the life of the shaft. This needs to be verified by physical experiments. Therefore, future research can be carried out by

constructing a physical model and obtaining the drawbacks of the model based on the experimental results and reusing the finite element software for optimisation.

References

Bianchi, N. and Bolognani, S. (1999) 'Performance analysis of an IPM motor with segmented rotor for flux-weakening applications', *IEEE Int. Conf. on Electrical Machines and Drives*, pp.49–53.

Bianchi, N., Bolognani, S. and Chalmers, B.J. (2000) 'Salient-rotor PM synchronous motors for an extended flux-weakening operation range', *IEEE Transactions on Industry Applications*, Vol. 36, No. 4, pp.1118–1125.

Boldea, I., Tutelea, L.N., Parsa, L. and Dorrell, D. (2014) 'Automotive electric propulsion systems with reduced or no permanent magnets: an overview', *IEEE Transactions on Industrial Electronics*, Vol. 61, No. 10, pp.5696–5711.

Chen, Y., Cai, T., Zhu, X., Fan, D. and Wang, Q. (2020) 'Analysis and design of a new type of less-rare-earth hybrid-magnet motor with different rotor topologies', *IEEE Transactions on Applied Superconductivity*, Vol. 30, No. 4, pp.1–6.

Dong, J., Gu, A., Yang, M. and Zhang, D. (2020) 'A method for improving torque performances of IPMSM', *IEEE Conference*, pp.1–6.

Du, L., Liu, X., Fu, J., Liang, J. and Huang, C. (2021) 'Design and optimization of reverse salient permanent magnet synchronous motor based on controllable leakage flux', *CES Transactions on Electrical Machines and Systems*, Vol. 5, No. 2, pp.163–173.

Ishii, S., Hasegawa, Y., Nakamura, K. and Ichinokura, O. (2012) 'Characteristics of novel flux barrier type outer rotor IPM motor with rare-earth and ferrite magnets', *IEEE Int. Conf. on Renewable Energy Research and Applications*, pp.1–4.

Islam, M.S., Islam, R. and Sebastian, T. (2014) 'Noise and vibration characteristics of permanent-magnet synchronous motors using electromagnetic and structural analyses', *IEEE Transactions on Industry Applications*, Vol. 50, No. 5, pp.3214–3222.

Kim, D., Jung, J., Hong, J., Kim, K. and Park, C. (2012) 'A study on the design process of noise reduction in induction motors', *IEEE Transactions on Magnetics*, Vol. 48, No. 11, pp.4638–4641.

Kimiabeigi, M., Widmer, J., Long, R. et al. (2015) 'High-performance low-cost electric motor for electric vehicles using ferrite magnets', *IEEE Transactions on Industrial Electronics*, Vol. 63, No. 1, pp.113–122.

Leitner, S., Gruebler, H. and Muetze, A. (2019) 'Cogging torque minimization and performance of the sub-fractional HP BLDC claw-pole motor', *IEEE Transactions on Industry Applications*, Vol. 55, No. 5, pp.4653–4664.

Liu, K., Zhang, B. and Feng, G. (2021) 'Research on electromagnetic vibration and noise characteristics of dual sided rotor permanent magnet synchronous motor based on armature offset approach', *Transactions of China Electrotechnical Society*, Vol. 36, pp.95–106.

Poudel, B., Amiri, E., Rastgoufard, P. and Mirafzal, B. (2021) 'Toward less rare-earth permanent magnet in electric machines: a review', *IEEE Transactions on Magnetics*, Vol. 57, No. 9, pp.1–19.

Qiu, Z., Chen, Y., Liu, X., Zhang, L. and Cheng, H. (2022) 'Evaluation and comparison of sideband harmonics and acoustic responses with continuous and discontinuous PWM strategies in permanent magnet synchronous motor for electric vehicles', *International Journal of Hydromechatronics*, Vol. 5, No. 2, pp.109–123.

Remus, N., Toulabi, M.S., Mukundan, S. et al. (2020) 'Electromagnetic noise and vibration in PMSM and their sources: an overview', *IEEE Int. Conf. on Electrical and Computer Engineering*, pp.1–4.

Sun, T., Kim, J., Lee, G., Hong, J. and Choi, M. (2011) 'Effect of pole and slot combination on noise and vibration in permanent magnet synchronous motor', *IEEE Transactions on Magnetics*, Vol. 47, No. 5, pp.1038–1041.

Wang, W., Wang, M., Guo, J., Liu, Y., Zheng, P. and Fu, Z. (2019) 'Multi-objective optimization of less-rare-earth interior permanent magnet synchronous machines used for electric vehicles', *IEEE Int. Conf. on Electrical Machines and Systems*, pp.1–5.

Wang, W., Zheng, P., Wang, M., Liu, Y., Fu, Z. and Sui, Y. (2018) 'Demagnetization and Permanent-Magnet Minimization Analyses of Less-Rare-Earth Interior Permanent-Magnet Synchronous Machines Used for Electric Vehicles', *IEEE Transactions on Magnetics*, Vol. 54, No. 11, pp.1–5.

Xing, Z., Zhao, W., Wang, X. and Sun, Y. (2020) 'Reduction of radial electromagnetic force waves based on PM segmentation in SPMSMs', *IEEE Transactions on Magnetics*, Vol. 56, No. 2, pp.1–7.

Yang, H. and Chen, Y. (2021) 'Influence of radial force harmonics with low mode number on electromagnetic vibration of PMSM', *IEEE Transactions on Energy Conversion*, Vol. 29, No. 1, pp.38–45.

Zeng, X., Xu, L. and Zhang, C. (2018) 'Design and optimization of a less-rare-earth permanent magnet brushless motor considering cost effective', *IEEE Int. Conf. on Electrical Machines and Systems*, pp.488–492.

Zheng, S., Zhu, X. and Xu, L. (2020) 'Optimization and comparison of two hybrid permanent magnet synchronous motors with contrary saliency characteristic', *IEEE Int. Conf. on Applied Superconductivity and Electromagnetic Devices*, pp.1–2.

Zheng, S., Zhu, X., Xu, L., Zhu, T. and Wu, D. (2021) 'Comparative analysis and multi-objective optimization of hybrid permanent magnet motors considering different saliency characteristics', *IEEE Transactions on Applied Superconductivity*, Vol. 31, No. 8, pp.1–5.

Zhu, X., Wu, W., Quan, L. et al. (2018) 'Design and multi-objective stratified optimization of a less-rare-earth hybrid permanent magnets motor with high torque density and low cost', *IEEE Transactions on Energy Conversion*, Vol. 34, No. 3, pp.1178–1189.

Zhu, X., Wu, W., Quan, L., Xiang, Z. and Gu, W. (2019) 'Design and multi-objective stratified optimization of a less-rare-earth hybrid permanent magnets motor with high torque density and low cost', *IEEE Transactions on Energy Conversion*, Vol. 34, No. 3, pp.1178–1189.